VI International Conference on Computational Methods for Coupled Problems in Science and Engineering
COUPLED PROBLEMS 2015
B. Schrefler, E. Oñate and M. Papadrakakis(Eds)

THREE-NODE ZERO-THICKNESS HYDRO-MECHANICAL INTERFACE FINITE ELEMENT FOR GEOTECHNICAL APPLICATIONS

B. CERFONTAINE*, A.C. DIEUDONNE*,†, J.P. RADU*, F. COLLIN* AND R. CHARLIER*

*Department ArGEnCo
University of Liege
B52, ULg, Liege, Belgium
e-mail: f.collin@ulg.ac.be

† FRIA - F.R.S. F.N.R.S
Brussels, Belgium

Key words: Interface, Numerical modelling, Finite elements, Offshore Engineering

Abstract. The paper presents the main features of a hydro-mechanical coupled finite element of interface. The mechanical problem accounts for the detection of contact, the development of contact pressure, shearing and relative sliding between two solids. A three-node discretisation of hydraulic problem allows the representation of fluid flow across and in the plane of the interface. The method involves a drop of pressure between each side of the interface and the inner medium. Hydro-mechanical couplings result from 1) the definition of the total pressure acting on each side of the interface according to the Terzaghi's principle; 2) the dependence of permeability on the gap opening; 3) the variation of the fluid mass stored within the gap.

1 INTRODUCTION

Interfaces play a crucial role in many fields of geotechnical engineering and engineering geology. Understanding their mechanism is necessary to deal with pile driving and design [1], the behaviour of faults in the vicinity of hydrocarbon production wells [2] and carbon dioxide geological sequestration [3], among others. In all these applications, hydro-mechanical couplings should be taken into account.
Suction caissons or bucket foundations are more and more installed as permanent foundations for offshore structures [4]. They consist of steel cylinders open towards the bottom and installed into the soil by suction. The role of interfaces is particularly crucial for their modelling, especially under pull loading [5, 6, 7].
Finite elements of interface were early developed [8] especially for the purpose of metal

forming [9]. However recent advances develop coupled finite elements taking into account fluid or gas phases [2, 10]. The main purpose of this work is to develop a finite element of interface able to reproduce the coupled hydro-mechanical behaviour in three dimensions and to apply it to the uplift modelling of a suction caisson. The element is implemented in the finite element code LAGAMINE, able to carry out fully coupled simulations [11].

2 INTERFACE ELEMENT

The finite element of interface involves two distinct but related issues: the mechanical and the flow problems. The mechanical problem tackles the detection of contact between two solids, the evolution of shearing and/or sliding. The flow problem describes fluid flows taking place inside and through the interface. These two problems are inherently interrelated. Fluid flow influences the pressure acting on each side of the interface. The mechanical opening/closing of the interface modifies its permeability and the mass of water stored inside. The extended definition of the interface element can be found in [12].

2.1 Mechanical problem

Let us consider two deformable porous media Ω^1 and Ω^2 in their current configuration in the global system of coordinates $(\mathrm{E}_1, \mathrm{E}_2, \mathrm{E}_3)$, as shown in Figure 1. In each point x_1 of the boundary Γ_c^1 where the contact between them is likely to happen, a local system of coordinate $(\mathbf{e}_1^1, \mathbf{e}_2^1, \mathbf{e}_3^1)$ can be defined such that $\mathbf{e}_1^1$ is normal to the boundary. The gap function g_N measures the distance between both solids. It is computed according to

$$\mathrm{g}_N = \left(\mathbf{x}^2 - \mathbf{x}^1\right) \cdot \mathbf{e}_1^1, \tag{1}$$

which is the closest-point projection of $\mathbf{x}^2$ onto $\mathbf{x}^1$. The gap function is generalised to each local tangential direction. However this definition has no meaning in the field of large displacements and the gap variation is defined instead [9] such that

$$\dot{\mathbf{g}} = \dot{g}_N \, \mathbf{e}_1^1 + \dot{g}_{T1} \, \mathbf{e}_2^1 + \dot{g}_{T2} \, \mathbf{e}_3^1. \tag{2}$$

When solids come into *ideal* contact, $\mathrm{g}_N = 0$, they deform and develop a contact pressure p_N since they cannot overlap each other. This condition is mathematically termed *contact constraint* or Hertz-Signorini-Moreau condition [13], it mathematically reads

$$\mathrm{g}_N \geq 0, \qquad \mathrm{p}_N \geq 0 \qquad \text{and} \qquad \mathrm{p}_N \, \mathrm{g}_N = 0. \tag{3}$$

If there is no contact, $\mathrm{g}_N > 0$ and contact pressure p_N is null. If contact takes place, $\mathrm{g}_N = 0$ and a contact pressure develops $\mathrm{p}_N \geq 0$. Shearing of the solids in contact gives birth to shear stresses (τ_1, τ_2) within the interface. They are defined in each local direction such that

$$\mathbf{t} = -\mathrm{p}_N \, \mathbf{e}_1^1 + \tau_1 \, \mathbf{e}_2^1 + \tau_2 \, \mathbf{e}_3^1. \tag{4}$$

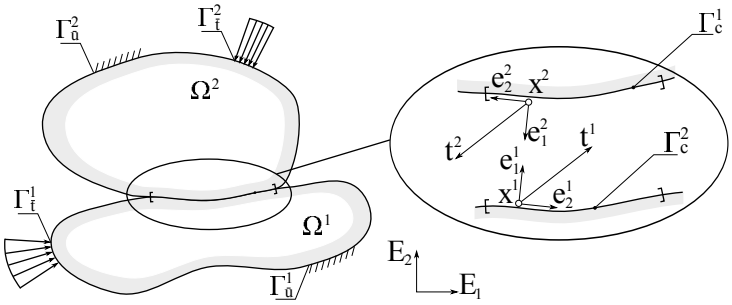

Figure 1: Statement of the mechanical problem, cross-section of the 3D problem in the $(\mathrm{E}_1, \mathrm{E}_2)$ plane: $\gamma_{\bar{u}}$, imposed displacements; $\gamma_{\bar{t}}$, imposed tractions.

The contact constraint defined by equation (3) is regularised by the penalty method. Therefore the contact is not ideal any more and interpenetration of both solids in contact is allowed, *i.e.* $\mathrm{g}_N < 0$. The evolution of normal pressure in case of contact reads

$$\dot{\mathrm{p}}_N = -\mathrm{K}_N \, \dot{\mathrm{g}}_N, \tag{5}$$

where K_N is a penalty coefficient and the minus sign ensures the contact pressure to be positive when interpenetration increases, *i.e.* $\dot{\mathrm{g}}_N < 0$.

In case of contact, both solids are either in ideal *stick* or *slip* state [13]. In the former, the relative displacement is equal to zero upon shearing. In the latter, the solids are allowed to move tangentially and the shear stress is limited to a maximum value. The transition between these states is ruled by the Mohr Criterion, such that

$$f(\mathbf{t}, \mu) = \underbrace{\sqrt{(\tau_1)^2 + (\tau_2)^2}}_{\|\tau\|} - \mu \, \mathrm{p}_N, \tag{6}$$

where μ is the friction coefficient. The stick state is also regularised by the penalty method. A small relative tangential displacement is allowed even in this case and the evolution of the shear stress is computed according to

$$\dot{\tau}_i = \mathrm{K}_T \, \dot{\mathrm{g}}_{Ti}, \tag{7}$$

where K_T is a tangential penalty coefficient. Therefore the evolution of the stress state within the interface is similar to the framework of elastoplasticity. The Coulomb criterion is the yield surface described in Figure 2, the elastic state is equivalent to the stick state and plasticity to slip state. Penalty coefficients $(\mathrm{K}_N, \mathrm{K}_T)$ are similar to elastic parameters even if they are introduced as purely numerical tools.

The finites elements developed belong to the family of zero-thickness elements. These elements lie on the boundary of the solids and have no thickness. They discretise the normal constraint and the shear stress along the boundary [8, 13]. The contact pressure and the gap function are computed at each integration point of one of the two solids, according to the mortar method [9, 14, 15]. The normal contact constraint is verified in a weak sense over the element.

	No contact	Stick	Slip
p_N	$= 0$	> 0	> 0
$\|\tau\|$	$= 0$	≥ 0	$= \mu \cdot p_N$

(a) Stress state in the interface in each case.

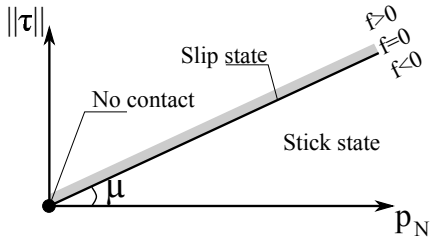

(b) Mohr-Coulomb criterion.

Figure 2: Analogy with elastoplasticity

2.2 Flow problem

Let us consider two solids that are porous media saturated with water. Therefore, depending on boundary conditions, fluid flow may take place within them as shown in Figure 3a. Solids Ω^1 and Ω^2 delineate a new volume Ω^3, which represents a discontinuity. Fluid flow may also exist along and through Ω^3.

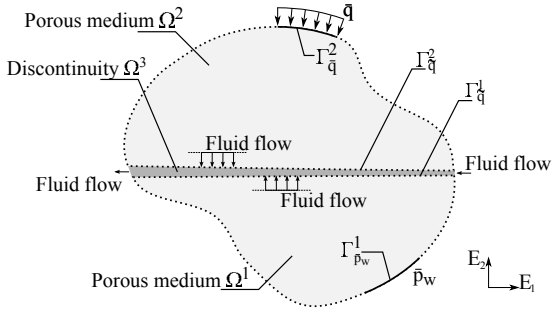

(a) Definition of the flow problem (cross section of the 3D case in the (E_1, E_2) plane), porous medium, discontinuity and boundaries: $\Gamma_{\bar{q}}$, imposed fluw; $\Gamma_{\bar{p}_w}$, imposed pressure.

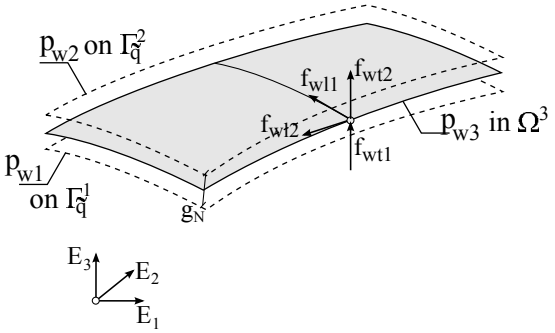

(b) Three-node discretisation: definition of longitudinal and transversal flows.

Figure 3

The interface is discretised according to a three-node scheme as shown in Figure 3b. The fields of water pressure are considered on each side of the interface ($\Gamma^1_{\bar{q}}, \Gamma^2_{\bar{q}}$) and inside it ($\Omega^3$). Therefore two longitudinal and two transversal fluxes must be respectively defined in the normal and tangential local directions.
Darcy's law is assumed to represent fluid flow in the local tangential directions such that

$$\mathrm{f}_{wl(i-1)} = -\frac{k_l}{\mu_w}\left(\nabla_{\mathbf{e}_i^1}\,\mathrm{p}_{w3} + \rho_w\,\mathrm{g}\,\nabla_{\mathbf{e}_i^1} z\right)\rho_w \qquad \text{for} \quad i = 2, 3 \tag{8}$$

where $\nabla_{\mathbf{e}_i^1}$ is the gradient in the direction $\mathbf{e}_i^1$, z is the vertical global direction, μ_w is the dynamic viscosity of the fluid, g the acceleration of gravity, ρ_w is the density of the fluid

and k_l is the longitudinal permeability.
The transversal fluid fluxes $(\mathrm{f}_{wt1}, \mathrm{f}_{wt2})$ between each side of the interface and the inner medium are defined according to

$$\mathrm{f}_{wt1} = \rho_w \, \mathrm{T}_{w1} \, (\mathrm{p}_{w1} - \mathrm{p}_{w3}) \qquad \text{on} \quad \Gamma^1_{\tilde{q}}, \tag{9}$$

$$\mathrm{f}_{wt2} = \rho_w \, \mathrm{T}_{w2} \, (\mathrm{p}_{w3} - \mathrm{p}_{w2}) \qquad \text{on} \quad \Gamma^2_{\tilde{q}}, \tag{10}$$

where T_{w1} and T_{w2} are two transversal conductivities.

2.3 Couplings

The mechanical and flow problems are intrinsically coupled. The total normal pressure acting on each side of the interface is decomposed according to Terzaghi's principle

$$\mathrm{p}_N = \mathrm{p}'_N + \mathrm{p}_{w3}. \tag{11}$$

where p'_N is the effective pressure and p_{w3} is the water pressure inside the interface. The Coulomb criterion becomes a function of the effective pressure only.

The opening/closing of the gap g_N has two effects. Firstly it influences the permeability of the discontinuity according to the cubic law [16, 2]

$$k_l = \begin{cases} \dfrac{(\mathrm{D}_0)^2}{12} & \text{if} \qquad \mathrm{g}_N \leq 0 \\ \dfrac{(\mathrm{D}_0 + \mathrm{g}_N)^2}{12} & \text{otherwise,} \end{cases} \tag{12}$$

where D_0 is the residual hydraulic aperture. If contact holds, i.e. $\mathrm{g}_N \leq 0$, it ensures that the permeability is not null. Indeed, if the surfaces of the bodies in contact are not perfectly smooth, there is still a residual opening. Finally the total mass of fluid M_f enclosed within the interface is modified according to

$$\dot{\mathrm{M}}_f = \left(\dot{\rho}_w \, \mathrm{g}_N + \rho_w \, \dot{\mathrm{g}}_N + \rho_w \, \mathrm{g}_n \, \frac{\dot{\Gamma}_{\tilde{q}}}{\Gamma_{\tilde{q}}} \right) \Gamma_{\tilde{q}}, \tag{13}$$

where $\Gamma_{\tilde{q}}$ is the total surface along which the water flow takes place. It is assumed that the tangential displacement remains limited $\dot{\Gamma}_{\tilde{q}} \to 0$ and the fluid is incompressible $\dot{\rho}_w = 0$.

2.4 Finite element discretisation

The final discretisation of a 3D interface is represented in Figure 4. Both sides of the interface are described by classical quadrangular isoparametric finite elements. Their nodes have four degrees of freedom, three mechanical and one fluid. Inner nodes have a single fluid degree of freedom since they only describe fluid flow.

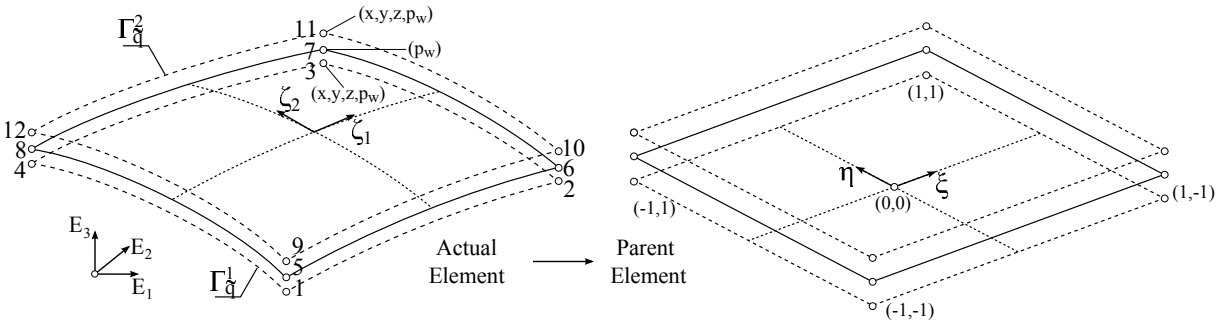

Figure 4: Discretisation of the interface into isoparametric elements. Transformation to the parent element.

3 APPLICATION

3.1 Statement of the problem

The application consists of the pull loading of a suction caisson embedded in an elastic layer of soil. This simulation is inherently 2D but a 3D simulation is carried out in order to check the formulation of the finite element. The caisson has an outer radius of 3.9m, an inner radius of 3.8m and a skirt length of 4m as shown in Figure 5a. The thickness of its lid and skirt are respectively 0.4m and 0.1m. Interface elements are set up between the soil and the caisson as described in Figure 5b.

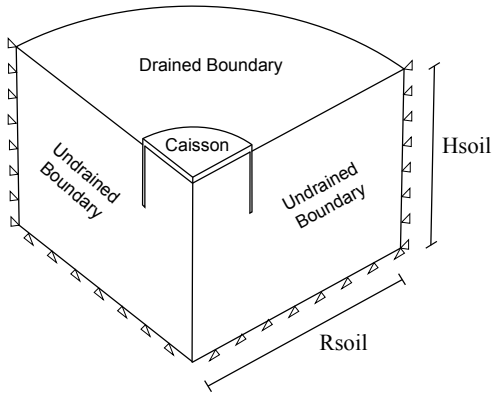

(a) Global sketch of the geometry of the problem.

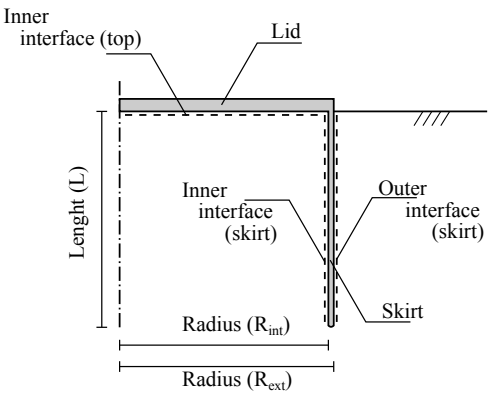

(b) Description of the caisson.

Figure 5

The caisson is made of steel and its behaviour is elastic. The elastic soil is represented by a quarter of cylinder. Its radius is equal to 24m and its depth to 12m. The soil is assumed elastic. All material parameters are provided in Table 1. Interface elements are characterised by a friction coefficient of 0.57. The transversal conductivity is equal to zero between the inner interface and the caisson since it is impervious. This conductivity

is equal to 1.E-8 m/Pa.s between the inner interface and the soil.

Two types of uplift simulations are carried out in order to validate the formulation of the three dimensional finite element. The first simulation is *drained*, *i.e.* there is no variation of pore pressures within the soil. It occurs if the loading rate is sufficiently low and pore pressures have time to dissipate. This simulation highlights the mechanical behaviour of the interface, *i.e.* the progressive mobilisation of friction along the skirt and the soil-caisson sliding. The second simulation is partially drained, pore pressures are able to partially dissipate. It illustrates the coupled behaviour of the interface element.

Soil	E [MPa]	ν [-]	n [-]	k [m^2]	γ_s [kg/m^3]	K_0 [-]
	2E2	0.3	0.36	1.E-11	2650	1
Caisson	E [MPa]	ν [-]	n [-]	k [m^2]	γ_s [kg/m^3]	K_0 [-]
	2E5	0.3	0.36	0	2650	1
Interface	K_N [N/m^3]	K_T [N/m^3]	μ [-]	D_0 [m]	T_w [m/(Pa.s)]	
	1E10	1E10	0.57	1.E-5	1.E-8	

Table 1: Material parameters: E Young modulus, ν Poisson's ratio, n porosity, k permeability, γ_s density of solid grains, K_0 coefficient of earth pressure at rest, K_N, K_T penalty coefficients, μ friction coefficient, T_w transversal conductivity, D_0 residual hydraulic aperture.

3.2 Drained simulation

During the displacement controlled simulation, the total uplifting load ΔF_{tot} is balanced by the dead weight and the shearing along the skirt (inside ΔF_{int} and outside ΔF_{ext}). Their evolution with respect to the vertical displacement is represented in Figure 6a. At the early beginning of the simulation, the evolution of ΔF_{int} and ΔF_{ext} is almost linear. Indeed, the Mohr criterion is not reached yet and the variation of the shear stress is a function of the variation of tangential displacement

$$\dot{\tau} = K_T \, \dot{g}_T. \tag{14}$$

The slopes of ΔF_{ext} and ΔF_{int} are different. Indeed, the soil plug inside the caisson moves upward with it, i.e. the caisson acts as a punch. Therefore the relative displacement is lower inside than outside.

Friction is progressively mobilised outside the caisson up to point A in Figure 6a. From this point the soil and the caisson start sliding at constant shear stress, leading to a plateau in the evolution of ΔF_{ext}. The mobilised friction outside the skirt, $\eta_{ext} = (\tau/p'_N)_{ext}$, is depicted in Figure 7a. The friction coefficient is reached along the whole outer skirt after an uplift displacement of 0.63mm.
It is worth noting the opening of a gap, denoted by $\eta_{ext} = 0$, at the top of the skirt.

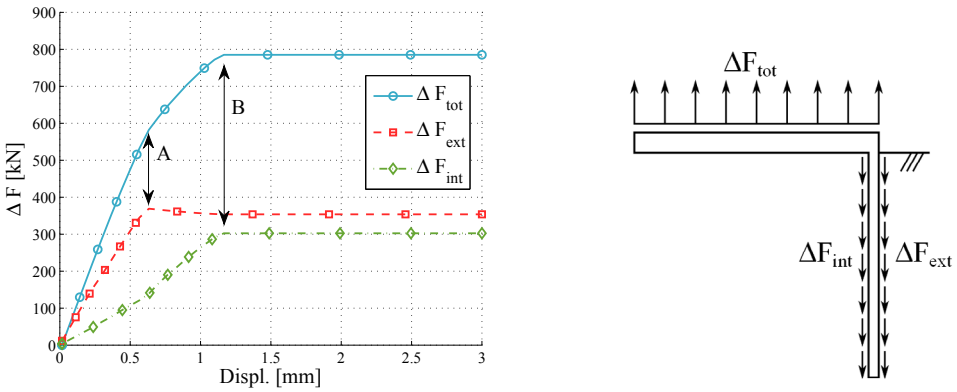

(a) (b)

Figure 6: Drained pull simulation of the suction caisson: ΔF_{tot} variation of total vertical load, ΔF_{ext} integral of shear mobilised outside the caisson, ΔF_{int} integral of shear mobilised inside the caisson.

Indeed, diffusion of shear stresses within the soil creates this loss of contact. This is mainly due to the elastic behaviour of the soil. Such a gap is strongly reduced if the soil has a non-linear elastoplastic behaviour [6, 17].
Similarly the outer friction is fully mobilised for a greater uplift displacement as shown in Figure 7b. The plateau is reached at point B in Figure 6a. The shear is more uniformly distributed and denotes the uplifting of the soil plug. The total applied load ΔF_{tot} reaches also a plateau since no additional friction can be mobilised. This plateau would not last for very large displacement. Indeed, the contact area decreases with increasing uplift.

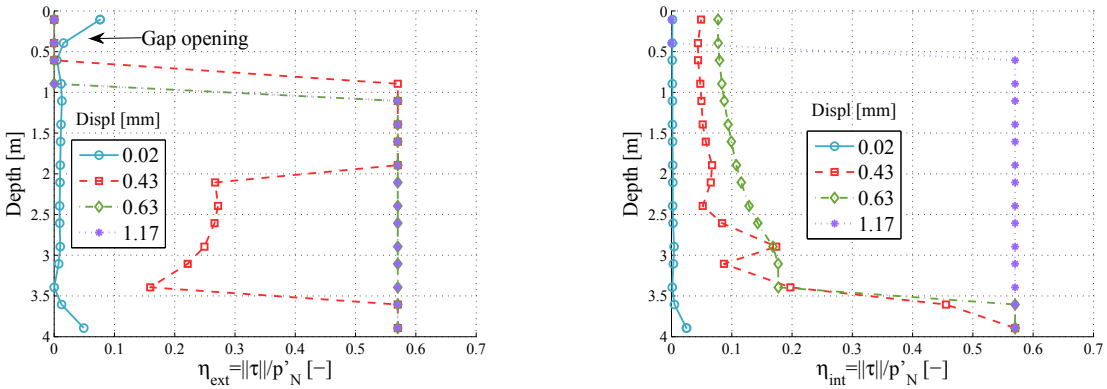

(a) Outside the caisson (η_{ext}). (b) Inside the caisson (η_{int}).

Figure 7: Drained pull simulation of the suction caisson, mobilised shear along the skirt.

3.3 Partially drained simulation

The partially drained uplifting of the caisson is illustrated in Figure 8a. In this case, the total load reached at the beginning of the plateau is greater than in the drained simulation. The suction effect involved in the installation of suction caissons is also mobilised during the uplift. The pull load creates an inverse consolidation process, where negative variations of pore pressures are generated inside the caisson. The differential of pressure between inside and outside holds the caisson. A new component of resistance is termed $\Delta \mathrm{F}_{uw}$. The distribution of variation of pore pressures, $\Delta \mathrm{p}_W$, is described in Figure 9a.

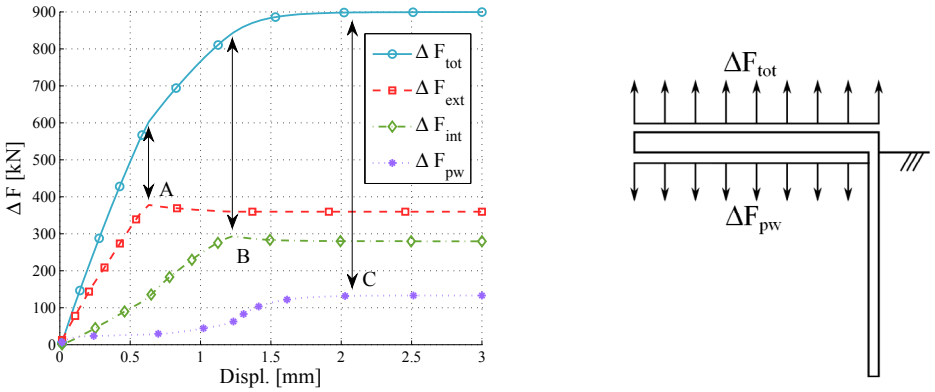

Figure 8: Undrained pull simulation of the suction caisson: $\Delta \mathrm{F}_{tot}$ variation of total vertical force, $\Delta \mathrm{F}_{ext}$ integral of shear mobilised outside the caisson, $\Delta \mathrm{F}_{int}$ integral of shear mobilised inside the caisson, $\Delta \mathrm{F}_{pw}$ integral of the variation of water pressure at the top inside the caisson.

The frictional behaviour is identical to the drained simulation. Friction is fully mobilised inside and outside the caisson at points A and B in Figure 8a. The last component of resistance $\Delta \mathrm{F}_{pw}$ starts increasing strongly after that point and finally reaches a plateau. The lid of the caisson and the soil plug keep in contact up to point A, as shown in Figure 8a. After sliding takes place on the outer skirt, a gap is opened between the lid and the soil. This gap is filled by water. Therefore, a transversal flux of water holds inside the caisson. The integral of the water flux over the top surface is provided in Figure 9b. The displacement of the top soil increases upward but reaches a plateau. After a displacement of 2mm, a stationary phase takes place. The upward displacement, the transversal flux and the variation of pressure are constant. If the caisson is assumed rigid, the rate of water stored within the gap is computed according to

$$\dot{\mathrm{S}} = \rho_w \, \mathrm{v}_{up} \, \pi \, \mathrm{R}_{int}^2 / 4 = 1.89 \, 10^{-1} \, \mathrm{kg/s}, \tag{15}$$

where v_{up} = 1mm/min is the uplifting rate. The mass variation is equal to the one numerically computed as observed in Figure 9b.

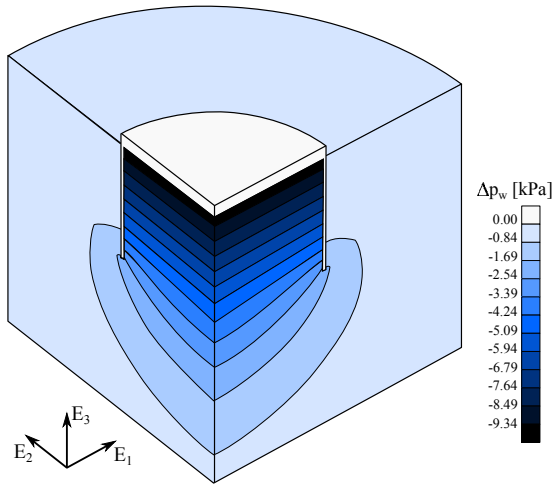

(a) Variations of pore water pressure Δp_w within the soil around the caisson, at the end of the simulation.

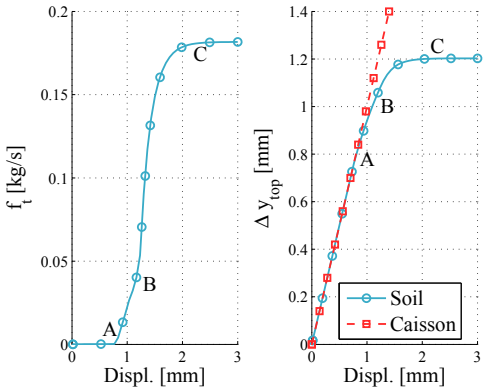

(b) Total transversal flux between the soil and the interface inside the caisson (left); vertical displacement of the top soil inside caisson.

Figure 9

The gap opening between the skirt and the soil, observed during the drained simulation, also occurs during the partially drained one. A longitudinal flow of water takes place within this gap. This is illustrated in Figure 10 at the end of the simulation. The flow is dependent on the gap opening since the permeability depends on the cubic law. This flow reduces the efficiency of the suction caisson since it decreases the length of the drainage path. However if an elastoplastic constitutive model was used, this pipe would be strongly reduced due to plasticity effects.

4 CONCLUSIONS

The main features of a finite element of interface are presented in this work. The element is zero-thickness. The normal contact constraint is regularised by the penalty method and discretised by the mortar approach. The discretisation of the hydraulic problem is three-node, namely the fluid flow inside the interface is discretised by additional nodes. Two longitudinal and two transversal fluxes are defined in the plane and across the interface.

The crucial role of interfaces is demonstrated for the simulation of the uplifting of a suction caisson. A first drained simulation is carried out. The maximum load sustainable by the suction caisson is bounded by the maximum friction available along the skirt. The caisson starts sliding afterwards.

The partially drained behaviour illustrates the coupled role of the interface element. The

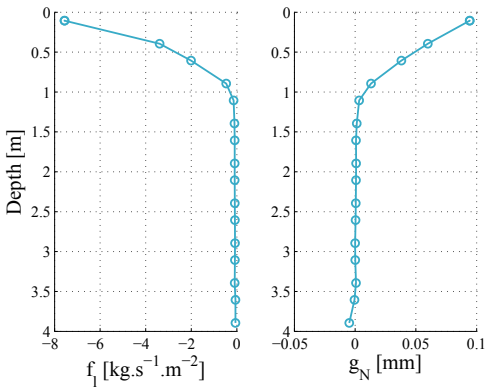

Figure 10: Relation between the longitudinal flux and the opening of a gap along the skirt, outside the caisson, end of the simulation.

inverse consolidation process taking place during the uplift generates negative variations of water pressures inside the caisson. This suction effect holds the caisson and transiently increases the total pulling load sustainable. The gap creating between the soil and the lid of the caisson is filled with water, illustrating the storage of of fluid within the interface. Longitudinal water flows also occur along the skirt due to the opening of a vertical gap. This reduces the effect of the suction caisson by reducing the length of the drainage path.

REFERENCES

[1] D. Sheng, P. Wriggers, and S.W. Sloan. Improved numerical algorithms for frictional contact in pile penetration analysis. *Computers and Geotechnics*, 33(6-7):341–354, September 2006.

[2] C. Guiducci, A. Pellegrino, J.-P. Radu, F. Collin, and R. Charlier. Numerical modeling of hydro-mechanical fracture behavior. In *Numerical models in Geomechanics*, 2002.

[3] J. Rutqvist, J.T. Birkholzer, and C.-F. Tsang. Coupled reservoir–geomechanical analysis of the potential for tensile and shear failure associated with co2 injection in multilayered reservoir–caprock systems. *International Journal of Rock Mechanics and Mining Sciences*, 45(2):132–143, 2008.

[4] G.T. Houlsby, L.B. Ibsen, and B.W. Byrne. Suction Caissons for Wind Turbines. *International Symposium on Frontiers in Offshore Geotechnics*, 75(September):94, 2005.

[5] K. Thieken, M. Achmus, and C. Schröder. On the behavior of suction buckets in sand under tensile loads. *Computers and Geotechnics*, 60:88–100, 2014.

[6] B. Cerfontaine, S. Levasseur, F. Collin, and R. Charlier. Axisymmetric transient modelling of a suction caisson in dense sand. In *Proceedings of the 8th European Conference on Numerical Methods in Geotechnical Engineering, NUMGE 2014*, volume 2, pages 1243–1248, 2014.

[7] B. Cerfontaine. *The cyclic behaviour of sand, from the Prevost model to offshore geotechnics*. PhD thesis, University of Liege, 2014.

[8] R.E. Goodman, R.L. Taylor, and T.L. Brekke. A model for the mechanics of jointed rock. *Journal of the Soil Mechanics and Foundations Division*, 94, 1968.

[9] A.M. Habraken, S. Cescotto, and Q. Banning. Contact between deformable solids: The fully coupled approach. *Mathematical and Computer modelling*, 28(4):153–169, 1998.

[10] B. Jha and R. Juanes. Coupled multiphase flow and poromechanics: A computational model of pore pressure effects on fault slip and earthquake triggering. *Water Resources Research*, 50:3376–3808, 2014.

[11] P. Gerard, R. Charlier, R. Chambon, and F. Collin. Influence of evaporation and seepage on the convergence of a ventilated cavity. *Water resources research*, 44(5), 2008.

[12] B. Cerfontaine, A.C. Dieudonné, J.P. Radu, F. Collin, and R. Charlier. 3d zero-thickness coupled interface finite element: formulation and application. *Computers and Geotechnics*, 2015 (submitted).

[13] P. Wriggers. *Computational contact mechanics*. Wiley : Chichester, second edition, 2006.

[14] M.A. Puso and T.A. Laursen. A mortar segment-to-segment contact method for large deformation solid mechanics. *Computer Methods in Applied Mechanics and Engineering*, 193(6):601–629, 2004.

[15] K.A. Fischer and P. Wriggers. Mortar based frictional contact formulation for higher order interpolations using the moving friction cone. *Computer methods in applied mechanics and engineering*, 195(37):5020–5036, 2006.

[16] R. Olsson and N. Barton. An improved model for hydromechanical coupling during shearing of rock joints. *International Journal of Rock Mechanics and Mining Sciences*, 38(3):317–329, 2001.

[17] B. Cerfontaine, F. Collin, and R. Charlier. Vertical transient loading of a suction caisson in dense sand. In *Proceedings of the 14th Int. Conference of International Association for Computer Methods and Recent Advances in Geomechanics, IACMAG 2014*, pages 929–934, 2015.